Am J Nucl Med Mol Imaging 2024;14(5):327-336
www.ajnmmi.us /ISSN:2160-8407/ajnmmi0159323

Original Article

Radiosynthesis and evaluation of a novel ^{18}F-labeled tracer for PET imaging of glycogen synthase kinase 3

Zhiwei Xiao[1,2*], Yinlong Li[1,2*], Ahmed Haider[1,2], Stefanie K Pfister[2], Jian Rong[1,2], Jiahui Chen[1,2], Chunyu Zhao[1,2], Xin Zhou[1], Zhendong Song[1], Yabiao Gao[1], Jimmy S Patel[1,3], Thomas L Collier[1,2], Chongzhao Ran[4], Chuangyan Zhai[1], Hongjie Yuan[5], Steven H Liang[1,2]

[1]Department of Radiology and Imaging Sciences, Emory University, Atlanta, GA 30322, USA; [2]Division of Nuclear Medicine and Molecular Imaging, Massachusetts General Hospital and Department of Radiology, Harvard Medical School, Boston, MA 02114, USA; [3]Department of Radiation Oncology, Winship Cancer Institute of Emory University, Atlanta, GA 30322, USA; [4]Athinoula A. Martinos Center for Biomedical Imaging, Department of Radiology, Massachusetts General Hospital and Harvard Medical School, Boston, MA 02114, USA; [5]Department of Pharmacology and Chemical Biology, Emory University School of Medicine, Atlanta, GA 30322, USA. [*]Equal contributors.

Received July 19, 2024, Accepted September 10, 2024; Epub October 15, 2024; Published October 30, 2024

Abstract: Glycogen synthase kinase 3 (GSK3) is a multifunctional serine/threonine kinase family that regulates diverse biological processes including glucose metabolism, insulin activity and energy homeostasis. Dysregulation of GSK3 is implicated in the development of several diseases such as type 2 diabetes mellitus, Alzheimer's disease (AD), and various cancer types. In this study, we report the synthesis and evaluation of a novel positron emission tomography (PET) ligand compound 28 (codenamed [^{18}F]GSK3-2209). The PET ligand [^{18}F]28 was obtained via copper-mediated radiofluorination in more than 32% radiochemical yields, with high radiochemical purity and high molar activity. *In vitro* autoradiography studies in rodents demonstrated that this tracer exhibited a high specific binding to GSK3. Furthermore, PET imaging studies of [^{18}F]28 revealed its ability to penetrate the blood-brain barrier (BBB).

Keywords: Glycogen synthase kinase 3, Alzheimer's disease, radiotracer, PET, ^{18}F-labeled

Introduction

Glycogen synthase kinase 3 (GSK3) is an intracellular serine/threonine kinase family that phosphorylates and inactivates glycogen synthase [1, 2]. This multifunctional enzyme is widely distributed in numerous tissues with peak levels found in the central nervous system (CNS) [3-5]. GSK3 regulates diverse biological processes such as cell metabolism [6], proliferation/differentiation [7], and synaptic neurotransmission [8], and is implicated in many human diseases including neurodegenerative pathologies [9], cardiovascular disorders [10], and various cancer types [11]. GSK3 consists of two highly homologous isozymes termed GSK3α (51 kDa) and GSK3β (47 kDa). These two isozymes show 98% amino acid sequence identity within their kinase domains and 84% overall identity but share only 36% similarity in the last 76 C-terminal residues [3, 12, 13]. Previous studies have shown that both isoforms are ubiquitously expressed at high levels in the brain but particularly enriched in the hippocampus, cerebral cortex, and cerebellum [14, 15]. Given the key role of GSK3 in tau hyperphosphorylation and other signaling pathways, aberrant GSK3 activity is associated with the pathogenesis of Alzheimer's disease (AD) [16], diabetes [17], and inflammation [18]. For instance, hyperactivity and/or overexpression of GSK3β has been observed in AD brains, leading to hyperphosphorylation of over 70% of potential phosphorylation sites on tau proteins, thereby disrupting their healthy association with microtubules [19]. Notably, GSK3 has emerged as a potential target for neurodegenerative and psychiatric drug development [20-22]. To date, despite among a variety of GSK3 inhibitors discovered some have reached clinical trials, including AZD1080 [23], Tideglusib [24], and LY2090314 [25], only lithium chloride (LiCl) [26] has been approved by the FDA. Notwithstanding the widespread use of lithium for bipolar disorders, limitations include a narrow therapeutic window, which required individual dose monitoring, as well as the potential to cause QT-prolongation. As such, there is an unmet medical need to provide alternative GSK3 inhibitors with an improved safety profile.

Positron emission tomography (PET) is a noninvasive *in vivo* nuclear medicine imaging modality that utilizes radioligands to characterize, visualize, and quantify physiological processes by recording time-dependent distribution in living organs [27]. Specifically, PET serves as a powerful tool for brain imaging, capable of measuring the aberrant activity and levels of GSK3 *in vivo* using a suitable PET radiotracer [28]. Various classes of GSK3 radiotracers have been recently reported to quantify the distribution of GSK3 in healthy and diseased states (**Figure 1**). For example, [^{11}C]AR-A014418 was the first reported radioligand for PET imaging of GSK3, but it exhibited limited blood-brain barrier (BBB) permeability [29]. Similarly, [^{11}C]

https://doi.org/10.62347/OBZS8887

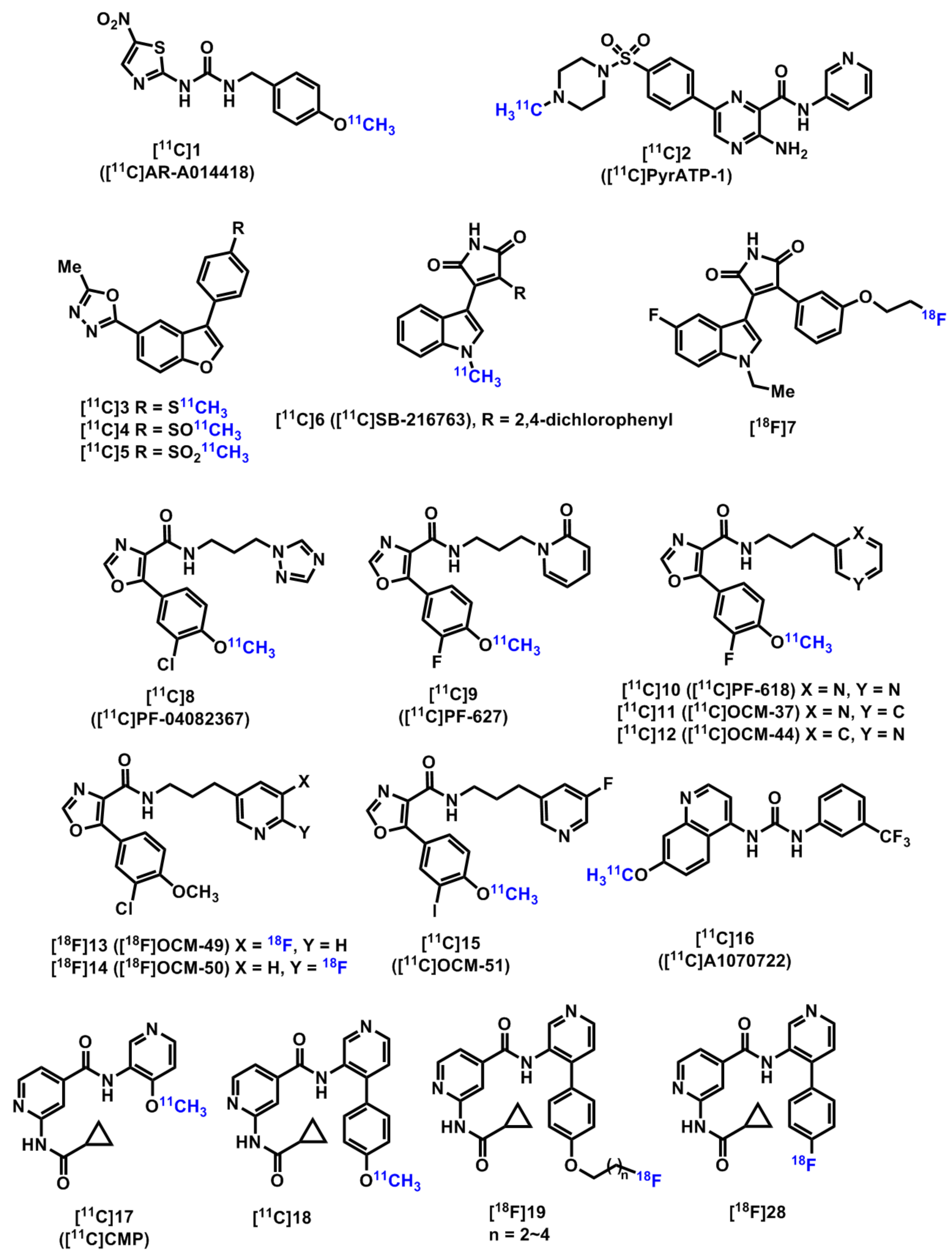

Figure 1. Representative radiotracers for GSK3 PET imaging.

PyrATP-1 (2) [30] and [[11]C]-oxadiazole-based radiotracers 3-5 demonstrated insufficient brain penetration *in vivo* [31]. Maleimide-derived tracers 6-7 showed promising preliminary results in BBB penetration and rodent brain uptake studies but require further evaluation in nonhuman primates [32-34]. [[11]C]PF-04802367 (8), one of the most potent and selective GSK-3 inhibitors, exhibited good uptake in brain regions with a homogeneous distribution [35]. Based on this finding, other ^{11}C and ^{18}F-labeled oxazole-4-carboxamide analogs 9-15 were developed, with [[11]C]OCM-44 showing promise for clinical translation [36, 37]. Recently, a series of isonicotinamide derivatives 17-19 were reported to have high affinity to GSK3β, but only [[18]F]19 showed reasonable brain uptake in GSK3β-rich regions [38-41]. Although imaging data in rats revealed unfavorable *in vivo* stability and specificity, in view of the heterogeneous brain uptake, there is high interest in developing of GSK3β radiotracers based on the structure of isonicotinamide derivatives. With this objective, we designed the synthesis and evaluation of a novel ^{18}F-labeled ligand [[18]F]28 for PET imaging of GSK3 in the brain of rodents. Preliminary physiochemical, in vitro binding properties, *in vivo* PET imaging, and metabolism studies were systematically investigated.

Materials and methods

General information

Unless noted, all the commercial chemicals, solvents, and biological samples were purchased and used directly without further purification. Aluminum TLC plates, 60 F_{254}, were employed for analytical thin-layer chromatography, visualizing with a 254 nm UV lamp. Flash column chromatography was conducted on 300-400 mesh silica gels. NMR spectra (^{1}H, ^{13}C, and ^{19}F) were obtained on Bruker 300 and 400 MHz spectrometers, with chemical shifts reported in parts per million (ppm) and coupling constants in Hertz. Imaging studies in rats were performed following the ethical rules of the Institutional Animal Care and Use Committee (IACUC) at Massachusetts General Hospital and Emory University. Mouse serum (mixed, Abcam, ab7486), rat serum (mixed, Abcam, ab7488), cynomolgus monkey serum (Abcam, ab155109), human serum (AB, male, Sigma-Aldrich, H4522), and mouse microsome (CD-1, Corning, 452701), rat microsome (SD, Corning, 452501), cynomolgus monkey microsome (Corning, 452411), human microsome (Corning, 452117) were purchased and used for *in vitro* stability test experiments and protein binding studies directly.

Chemical synthesis

The standard compound and the corresponding precursor were synthesized in five steps, respectively. The detailed reaction conditions and characterizations are shown below (see NMR spectrum in Supplementary Materials).

methyl 2-(cyclopropanecarboxamido)isonicotinate (22): To a solution of compound 21 (3.00 g, 19.7 mmol, 1.00 eq) and cyclopropanecarboxylic acid (1.87 g, 21.7 mmol, 1.72 mL, 1.10 eq) in DCM (40.0 mL) was added T_3P (18.8 g, 29.6 mmol, 17.6 mL, 50% purity, 1.50 eq) and DIEA (10.2 g, 78.6 mmol, 13.7 mL, 4.00 eq). The mixture was stirred at 25°C for 5 h, and the progress of the reaction was monitored and indicated by the TLC (Petroleum ether:Ethyl acetate = 3:1, R_f = 0.35) and LC-MS. LCMS (ESI): m/z = 221.1 $[M+H]^+$. The reaction mixture was concentrated under vacuum, and the residue was purified by flash column chromatography (SiO_2, Petroleum ether/Ethyl acetate = 100/1 to 3/1). Compound 22 (2.10 g, 9.53 mmol, 48.3% yield) was obtained as a white solid and used without further purification.

2-(cyclopropanecarboxamido)isonicotinic acid (23): To a solution of compound 22 (2.10 g, 9.53 mmol, 1.00 eq) in THF (20.0 mL) and H_2O (10.0 mL) was added LiOH•H_2O (600 mg, 14.3 mmol, 1.50 eq). After stirring at 25°C for 2 h, LC-MS indicated that 4.96% of compound 22 remained, and desired compound mass was detected. LCMS (ESI): m/z = 207.1 $[M+H]^+$. The solvent THF was removed under vacuum, and the aqueous was washed with DCM (30 mL) and adjusted to pH = 2-3 with aq. HCl (1 M). After extracted with DCM (30 mL × 2), the organic phase was concentrated under vacuum to give compound 23 (1.50 g, 7.27 mmol, 76% crude) as a white solid. ^{1}H NMR (400 MHz, DMSO-d_6): δ 8.55 (s, 1H), 8.43 (d, J = 4.8 Hz, 1H), 7.47 (dd, J_1 = 4.8 Hz, J_2 = 1.6 Hz, 1H), 2.04 - 1.99 (m, 1H), 0.87 - 0.75 (m, 4H).

2-(cyclopropanecarboxamido)-N-(4-(4-(4,4,5,5-tetramethyl-1,3,2-dioxaborolan-2-yl)phenyl)pyridin-3-yl)isonicotinamide (24): To a solution of compound 23 (500 mg, 2.43 mmol, 1.00 eq) and 4-(4-(4,4,5,5-tetramethyl-1,3,2-dioxaborolan-2-yl)phenyl)pyridin-3-amine (575 mg, 1.94 mmol, 0.80 eq) in DCM (5.00 mL) was added TEA (983 mg, 9.70 mmol, 1.35 mL, 4.00 eq) and CMPI (930 mg, 3.63 mmol, 1.50 eq). The mixture was stirred at 45°C for 12 h, and the progress of the reaction was monitored and indicated by the TLC (Petroleum ether:Ethyl acetate = 1:1, R_f = 0.29) and LC-MS. LCMS (ESI): m/z = 485.4 $[M+H]^+$. The reaction mixture was concentrated under reduced pressure and purified by prep-TLC (SiO_2, DCM:MeOH = 10:1) to give compound 24 (230 mg, 435 umol, 18.0% yield, 91.7% purity) as a yellow solid. ^{1}H NMR (400 MHz, $CDCl_3$): δ 9.60 (s, 1H), 8.52 (d, J = 5.2 Hz, 1H), 8.49 (s, 1H), 8.38 (d, J = 5.2 Hz, 1H), 8.32 (brs, 1H), 8.14 (s, 1H), 7.99 (d, J = 8.4 Hz, 2H), 7.48 (d, J = 8.0 Hz, 2H), 7.40 (dd, J_1 = 5.2 Hz, J_2 = 1.6 Hz, 1H), 7.26 (s, 1H), 1.61 - 1.54 (m, 1H), 1.38 (s, 12H), 1.23 - 1.16 (m, 2H), 0.97 - 0.90 (m, 2H).

4-(4-fluorophenyl)-3-nitropyridine (26): A mixture of 4-chloro-3-nitropyridine 25 (2.0 g, 12.62 mmol, 1.0 equiv), 4-fluorophenylboronic acid (18.92 mmol, 1.5 equiv) and Na_2CO_3 (3.34 g, 31.54 mmol, 2.5 equiv),

$Pd(Ph_3)_2Cl_2$ (442.8 mg, 0.631 mmol, 0.05 equiv) in toluene/ethanol/H_2O (40/8/16 mL) was degassed. After being stirring at 100°C for 4 h, the reaction mixture was poured into a saturated aqueous $NaHCO_3$ solution, and extracted with ethyl acetate 3 times. The combined organic layers were washed with brine, dried over $MgSO_4$, and concentrated under reduced pressure. The residue was purified by column chromatography (PE/EA = 2/1) to give compound 26 as a yellow solid in 88% yield. Melting point: 96-97°C. ^{1}H NMR (300 MHz, $CDCl_3$): δ 9.07 (s, 1H), 8.80 (d, *J* = 5.1 Hz, 1H), 7.38 (dd, *J* = 5.0, 0.5 Hz, 1H), 7.36 - 7.27 (m, 2H), 7.22 - 7.10 (m, 2H). ^{19}F NMR (282 MHz, $CDCl_3$): δ -106.78 - -106.94 (m). ^{13}C NMR (75 MHz, $CDCl_3$): δ 163.66 (d, *J* = 250.6 Hz), 152.92, 145.60, 145.38, 143.06, 130.58 (d, *J* = 3.5 Hz), 129.80 (d, *J* = 8.5 Hz), 125.85, 116.42 (d, *J* = 22.1 Hz).

4-(4-fluorophenyl)pyridin-3-amine (27): A mixture of compound 26 (12.62 mmol) and 10% Pd/C (1.35 g) in methanol (80 mL) and ethyl acetate (80 mL) was stirred under H_2 at 1 atm for 3 h. The catalyst was removed by filtration through a pad of Celite. The clear solution was concentrated to give compound 27 as a white solid in 99% yield. Melting point: 84-85°C. ^{1}H NMR (300 MHz, DMSO): δ 7.99 (d, *J* = 84.9 Hz, 2H), 7.64 - 6.85 (m, 5H), 5.12 (s, 2H). ^{19}F NMR (282 MHz, DMSO): δ -110.27. ^{13}C NMR (75 MHz, DMSO): δ 161.71 (d, *J* = 244.7 Hz), 141.45, 137.93, 137.78, 133.47 (d, *J* = 3.3 Hz), 130.36 (d, *J* = 8.3 Hz), 130.22, 123.92, 115.77 (d, *J* = 21.3 Hz).

2-(2-cyclopropyl-2-oxoethyl)-N-(4-(4-fluorophenyl)pyridin-3-yl)isonicotinamide (28): To a solution of the 23 (0.315 mmol, 1.0 equiv) and 27 (0.315 mmol, 1.0 equiv) in DMF (1.1 mL) was added T_3P (601.4 mg, 0.945 mmol, 3.0 equiv). After stirring at room temperature overnight, the reaction mixture was poured into a saturated aqueous $NaHCO_3$ solution and extracted with ethyl acetate 3 times. The combined organic layers were washed with water and brine, dried over anhydrous Na_2SO_4, and concentrated. The residue was purified by column chromatography (EA) to give the desired product as a white solid in 59% yield. ^{1}H NMR (300 MHz, $CDCl_3$): δ 9.57 (s, 1H), 8.57 (s, 1H), 8.51 (d, *J* = 5.0 Hz, 1H), 8.42 - 8.34 (m, 2H), 8.09 (s, 1H), 7.49 - 7.38 (m, 3H), 7.29 - 7.23 (m, 3H), 1.57 (tt, *J* = 7.7, 4.5 Hz, 1H), 1.19 - 1.07 (m, 2H), 0.98 - 0.89 (m, 2H). ^{19}F NMR (282 MHz, $CDCl_3$): δ -107.39 (ddd, *J* = 14.5, 9.1, 5.4 Hz). ^{13}C NMR (75 MHz, $CDCl_3$): δ 172.74, 163.62, 163.41 (d, *J* = 249.8 Hz), 152.50, 149.21, 146.16, 144.03, 143.52, 140.33, 131.44, 131.18 (d, *J* = 3.5 Hz), 130.46 (d, *J* = 8.5 Hz), 124.56, 117.96, 117.32 (d, *J* = 21.9 Hz), 110.19, 15.99, 8.90.

Radiosynthesis of [^{18}F]28

After generated via the ^{18}O(*p*,*n*)^{18}F reaction, [^{18}F]F^- was trapped on a Sep-Pak QMA cartridge which was pre-conditioned with 10 mL of 7.5% aqueous $NaHCO_3$ and 20 mL of H_2O. The [^{18}F]fluoride was eluted into a v-vial with a solution of $TEAHCO_3$ (0.5 mg) in MeOH (1.0 mL) and then dried under N_2 flow at 110°C for 10 min. To produce [^{18}F]28, 2.0 mg precursor, 7.0 mg $Cu(OTf)_2(pyridine)_4$ and 300 μL DMAc/^{n}BuOH (2/1) were transferred into the vial. After heated at 90°C for 20 min under air atmosphere, the solution was diluted with a CH_3CN/H_2O HPLC mobile phase to 3 mL, and then loaded into a semi-preparative radio-performance liquid chromatography (radio-HPLC) system equipped with a Phenomenex Luna 5μ C18 column (10 mm × 250 mm).Mobile phase of CH_3CN/H_2O = 30/70 (0.1%Et_3N) was used at a 5 mL/min flow rate, and UV at 254 nm. The retention time of [^{18}F]28 was 19.6 min. The radiotracer collected was further purified with a Sep-Pak C18 light cartridge and tested on an analytical HPLC system using a Bridge (4.6 mm × 150 mm) column and mobile phase of CH_3CN/H_2O = 30/70 (0.1%Et_3N) at a 1 mL/min flow rate. The non-decay-corrected radiochemical yield was 32% (25.1 mCi) EOB with >99% radiochemical purity with more than 1 Ci/μmol molar activity.

In vitro stability analysis in serum and liver microsome

Serum stability. 400 μL of serum for each species was added into a 1.5 mL Eppendorf tube and pre-incubated at 37°C for 5 minutes. After [^{18}F]28 was added (20 μL/300 μCi), the mixture was incubated at 37°C. After 30 and 60 mins, 100 μL samples were drawn out and stopped with ice-cold CH_3CN. Each sample was then centrifuged at 10,000 g for 5 min and analyzed by an analytical HPLC system equipped with an X-Bridge Phenyl column (4.6 mm × 100 mm, 5 *μ*m) with a mobile phase of CH_3CN/H_2O = 50/50 (0.1%Et_3N) at a 1 mL/min flow rate.

Liver microsome stability. A mixture of 340 μL of potassium phosphate buffer solution (0.5 M, pH 7.4), 40 μL of NADPH regenerating solution (10 mM) and 10 μL of radiotracer formulation was pre-incubated at 37°C for 5 minutes. 10 μL of liver microsome was then added. At the following time points, 30 and 60 mins, 100 μL samples were taken out and disposed as described above.

Protein binding test

To a solution of 150 μL serum in an Eppendorf tube was added a radiotracer formulation (10 μL/30 μCi). After being incubated at 37°C for 10 mins, the radiotracer-plasma solution was diluted with 300 μL of ice-cold PBS. The samples were vortexed briefly and centrifuged at 14,000 g in Amicon centrifugal filters with a size cutoff of 3 kDa for 15 min at 4°C. 200 μL × 2 of PBS was then used to wash the Eppendorf tube and centrifuged with the filter. The radioactivity of the filter and filtrate was measured in a gamma counter. The free fraction of radiotracer in plasma was the calculated according to the following equation:

$$f = A_{free}/(A_{protein}+A_{free})$$

PET imaging

Rodents PET imaging studies were performed with Sprague Dawley rats (female, body weight 195-282 g). A

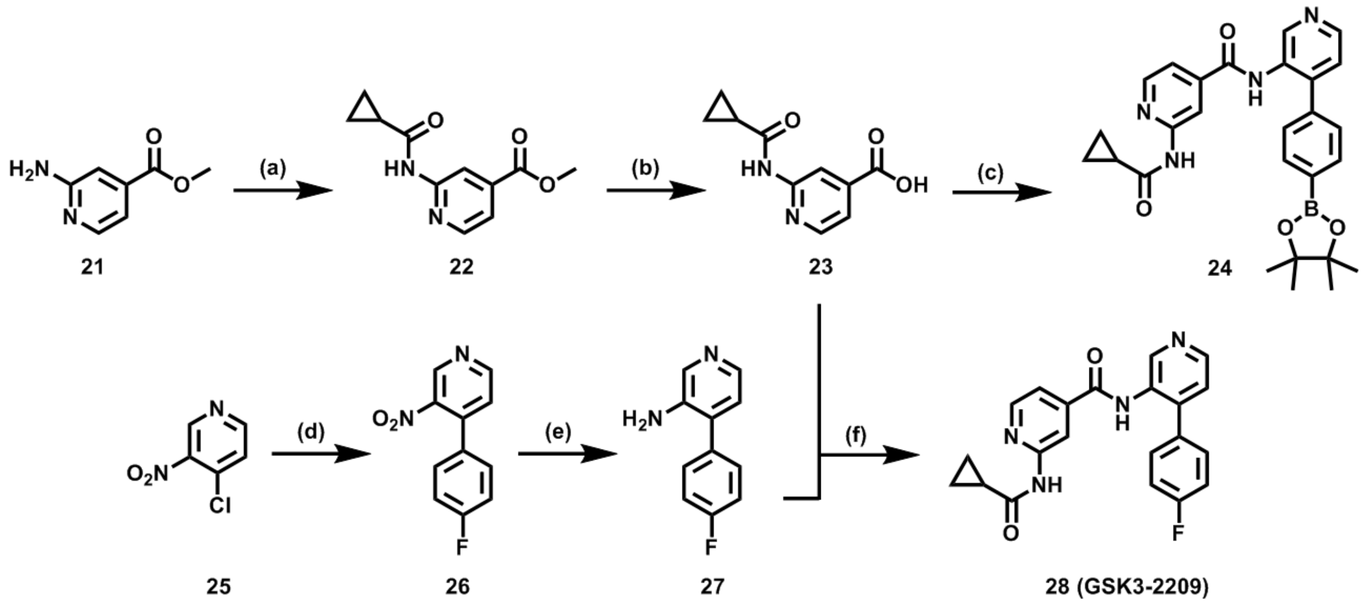

Figure 2. Synthesis of standard compound and the corresponding precursor. Reagents and reaction conditions. (a) cyclopropanecarboxylic acid, T_3P, DIPEA, DCM, RT, 5 h; (b) LiOH, THF/H_2O, RT, 2 h; (c) 2-chloro-1-methylpyridinium iodide (CMPI), 4-(4-(4,4,5,5-tetramethyl-1,3,2-dioxaborolan-2-yl)phenyl)pyridin-3-amine, TEA, DCM, 45°C, 12 h; (d) 4-fluorophenylboronic acid, Na_2CO_3, $Pd(Ph_3)_2Cl_2$, toluene/ethanol/H_2O, 100°C, 4 h; (e) 10% Pd/C, methanol/ethyl acetate, RT, 3 h; (f) T_3P, DMF, RT, overnight.

60 mins dynamic scan of the whole body for mice and whole brain for rats was performed, respectively. The rodents were kept under anesthesia with isoflurane during the entire scan. The radiotracer formulation and blocking inhibitor solution were injected via the tail vein. For mice, PET scans started immediately after the co-administration of radiotracers and the inhibitors. For rats, the PET scans started 5 min later after the co-administration. For blocking studies, non-radiolabeled reference compound 28 (3 mg/kg) and PF-04802367 (3 mg/kg and 1 mg/kg) were administered.

Results and discussion

Chemical synthesis

Despite the remarkable potency and selectivity ([^{11}C]CMP, IC_{50} = 3.4 nM; [^{18}F]19, IC_{50} = 1.4-3.3 nM), the lack of metabolic stability in rodents has hindered the clinical utility of isonicotinamide scaffolds as GSK3-specific tracers [38]. To enhance *in vivo* stability and lipophilicity, a C(sp^2)-F structured isonicotinamide scaffold was selected as a benchmark compound. An arylboronic ester derivative was then synthesized as the corresponding precursor compound using oxidative radiofluorination labeling methodology. According to literature procedures [39], we designed and synthesized both the reference compound 28 (reported GSK-3β/α IC_{50}: 5.2/1.7 nM) [42] and the corresponding precursor compound 24 from the same key intermediate compound 23 (**Figure 2**). This intermediate was synthesized from commercially available methyl 2-aminoisonicotinate in two steps, yielding moderate yields of 48% and 76%, respectively. The corresponding precursor compound 24 was obtained through the esterification reaction of compound 23 and 4-(4-(4,4,5,5-tetramethyl-1,3,2-dioxaborolan-2-yl)phenyl) pyridin-3-amine in 18% yield. For the synthesis of reference compound GSK3-2209, Suzuki coupling reactions of commercially available 4-chloro-3-nitropyridine and 4-fluorophenylboronic acid gave the compound 26 in 88% yield, which further converted to intermediate compound 27 by nitro-reduction reaction with palladium/activated carbon in 99% yield. Subsequently, the reference compound GSK3-2209 was obtained in 59% yield through the esterification reaction of intermediate 23 and 27.

Radiochemistry and in vitro characterization

The radiosynthesis of [^{18}F]28 was performed utilizing the oxidative radiofluorination methodology with the Bpin precursor, 2-(cyclopropanecarboxamido)-N-(4-(4-(4,4,5,5-tetramethyl-1,3,2-dioxaborolan-2-yl)phenyl)pyridin-3-yl) isonicotinamide (24). Cyclotron-produced [^{18}F]fluoride was dried under nitrogen flow in the presence of tetraethylammonium bicarbonate ($TEAHCO_3$) for 20 minutes. Subsequently, a mixture of Bpin precursor (24) (2.0 mg), $Cu(OTf)_2(pyridine)_4$ (7.0 mg), $TEAHCO_3$ (0.5 mg), and 300 μL DMAc/^{n}BuOH (2/1) was heated at 90°C for 20 minutes under air atmosphere (**Figure 3A**). After purified by a semi-preparative radioHPLC system, the collected fraction was diluted with sterile water and trapped with a light C18 cartridge. It was then formulated with ethanol and PBS. [^{18}F]28 was ultimately obtained in a non-decay-corrected radiochemical yield of 32% (25.1 mCi) with >99% radiochemical purity and greater than 1.0 Ci/μmol molar activity at 90 minutes EOB. *In vitro* formulation stability assay

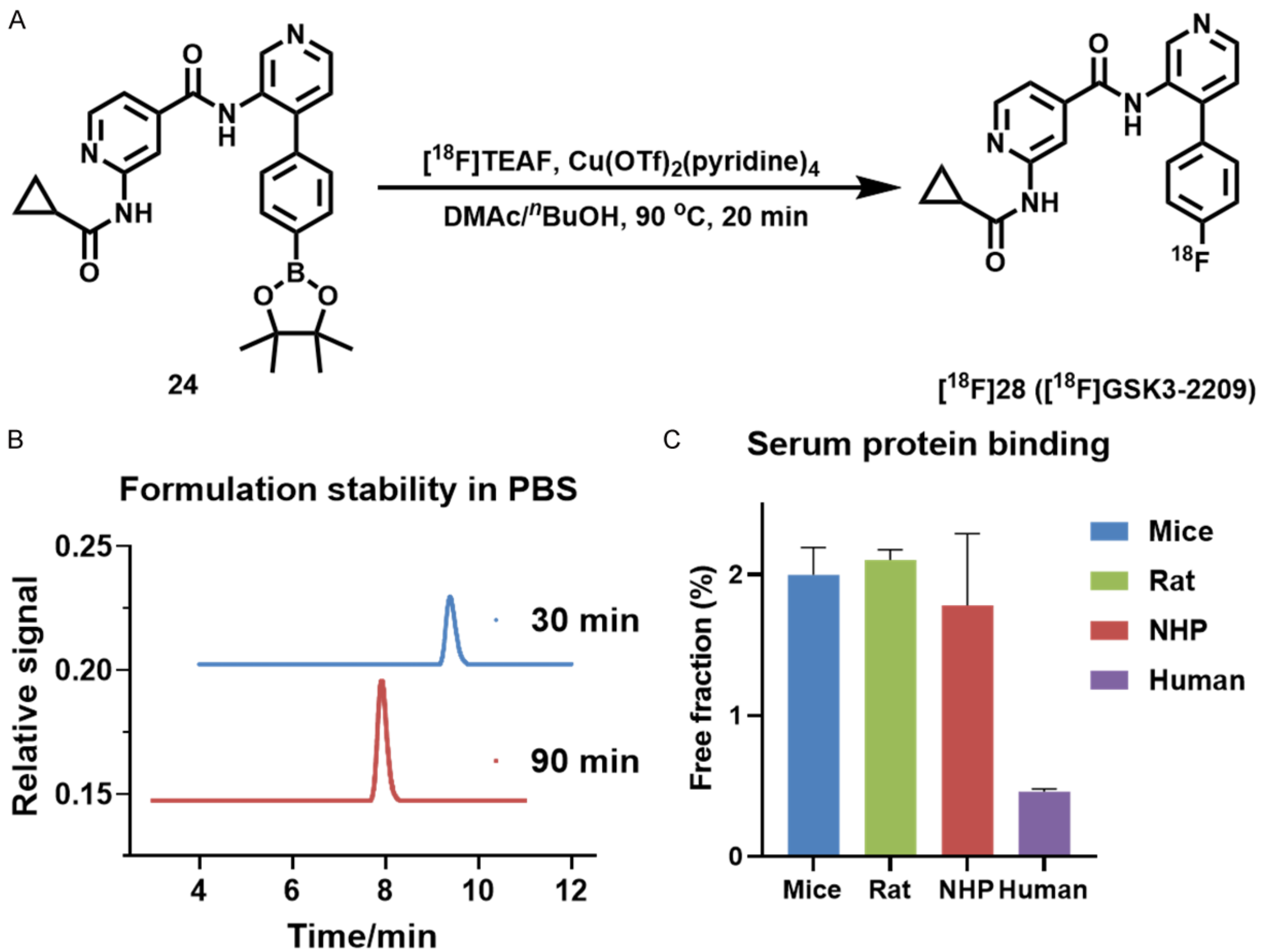

Figure 3. A. Radiosynthesis of [^{18}F]28; B. Formulation stability of [^{18}F]28 in PBS at 30 mins and 90 mins; C. Free fraction of [^{18}F]28 in serum.

revealed that more than 99% of intact [^{18}F]28 remained in PBS after 90 minutes (**Figure 3B**).

To assess the *in vitro* metabolic stability of [^{18}F]28, co-incubation of [^{18}F]28 and plasma and liver microsome was conducted. The radiometabolites were analyzed using a radio-HPLC system at 30 and 60 minutes time points (**Figure 4A**). Across all four species studied, mice, rats, NHPs and humans, [^{18}F]28 demonstrated excellent *in vitro* stability. 60 minutes after co-incubation with mouse and rat plasma, over 90% of the parent tracers remained intact, while over 99% remained in NHPs and humans. Notably, significant species differences were observed in liver microsomes. Specifically, [^{18}F]28 exhibited the highest stability in rats, with the unmetabolized parent fraction reaching 96% and 92% at 30 and 60 minutes, respectively (**Figure 4B**). In mice, only 68% and 54% parent tracer remained at 30 and 60 minutes, respectively, indicating that rats are more suitable candidates for PET imaging studies with [^{18}F]28. Furthermore, considering the distinct difference between human (90% at 30 minutes and 89% at 60 minutes) and NHPs (78% at 30 minutes and 65% at 60 minutes), it is conceivable that [^{18}F]28 would reveal better potentials in higher species. Following co-incubation of the tracer with plasma, the plasma free fraction (f_p) of [^{18}F]28 was determined to be 2.0%, 2.1%, 1.8%, and 0.5% in mice rats, NHPs and humans respectively (**Figure 3C**). Furthermore, employing the shake flask method, the $LogD_{7.4}$ value of [^{18}F]28 was determined to be 2.77±0.01.

PET imaging studies in rats

Encouraged by the promising *in vitro* stability in plasma and liver microsomes, dynamic microPET imaging study (0-60 mins) was conducted to evaluate the *in vivo* brain biodistribution and clearance of [^{18}F]28 (**Figure 5A**). Time-activity curves (TACs) in mice showed rapid uptake of [^{18}F]28 with SUV_{peak} appearing at 1 minute (Figure S1), suggesting BBB permeability. In view of the excellent *in vitro* stability of [^{18}F]28 in rats, dynamic PET imaging of whole brain in female SD rats was then carried out. TACs in rats showed the BBB permeability of [^{18}F]28 and a higher accumulation in brain (SUV = 0.51±0.04, n = 3 vs

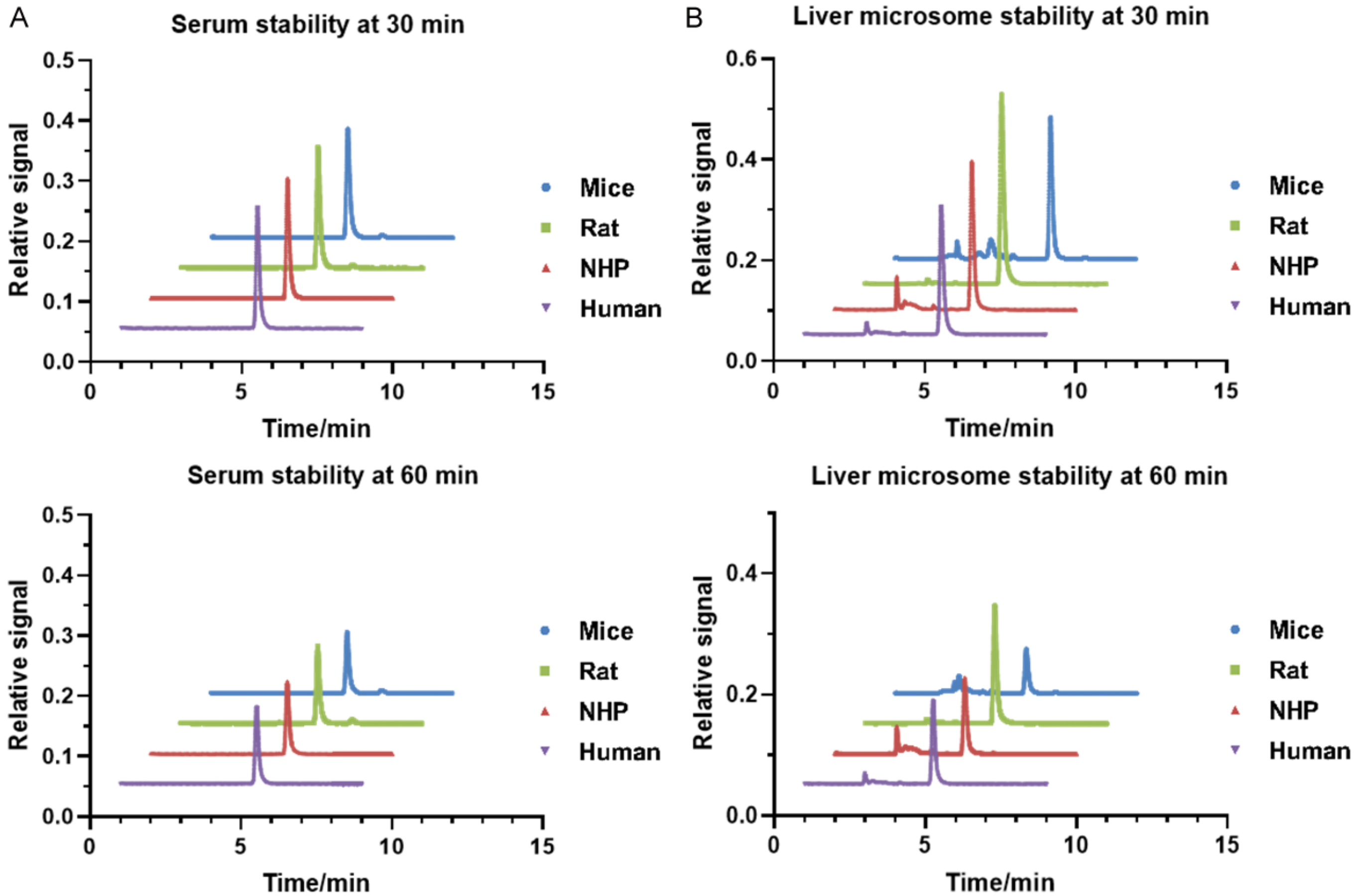

Figure 4. A. Serum stability after co-incubation for 30 mins and 60 mins; B. Liver microsome stability of [^{18}F]28 at 30 mins and 60 mins.

0.30±0.03, n = 4 at 25 mins, respectively). No upturning of the TACs throughout the whole 60 minutes scan was observed, and a suitable washout rate suggested the potential value of [^{18}F]28 for GSK3-targeted imaging. Despite the higher uptake under baseline condition (SUV = 0.51±0.04, n = 3 vs 0.35±0.05, n = 3 at 25 mins, respectively), [^{18}F]28 showed a homogeneous distribution across distinct brain regions, including cortex, hippocampus, stratum, and cerebellum (SUV = 0.52±0.03, 0.53±0.08, 0.53±0.04, and 0.49±0.07, respectively). Blocking studies using PF-04802367 showed visible reduction (32%) of brain uptake as shown in **Figure 5B**, indicating moderate level of specific binding in the brain.

Conclusion

Despite GSK3 is addressed to be implicated in many human diseases, there is an unmet medical need of GSK3 targeted inhibitors, due to the lack of specific probes. To better understand the role of GSK3 in related diseases, visualize and quantify GSK3 expression noninvasively, in this study, we have designed and synthesized a novel GSK3 targeted radiotracer based on an isonicotinamide core structure. Utilizing a one-pot oxidative radiofluorination methodology, [^{18}F]28 was successfully synthesized in excellent non-decay-corrected radiochemical yield of 32% and high radiochemical purity. Through *in vitro* evaluations, [^{18}F]28 exhibited nanomolar affinity and demonstrated exceptional stability. Dynamic PET imaging studies indicated suitable BBB permeability and brain kinetics of [^{18}F]28 for GSK3-targeted PET imaging. These findings collectively suggest the potential utility of isonicotinamide scaffolds as GSK3 specific tracers. However, given the significant species difference, further evaluation of [^{18}F]28 in higher species, especially in disease settings including AD, diabetes and cancer, is necessary to investigate its brain kinetics and specific binding.

Acknowledgements

We thank the Division of Nuclear Medicine and Molecular Imaging, Radiology, MGH and Harvard Medical School, and Department of Radiology and Imaging Sciences, Emory University School of Medicine for general support. S.H.L. gratefully acknowledges the support provided, in part, by the NIH grant (AG081401), Emory Radiology Chair Fund, and Emory School of Medicine Endowed Directorship.

Disclosure of conflict of interest

None.

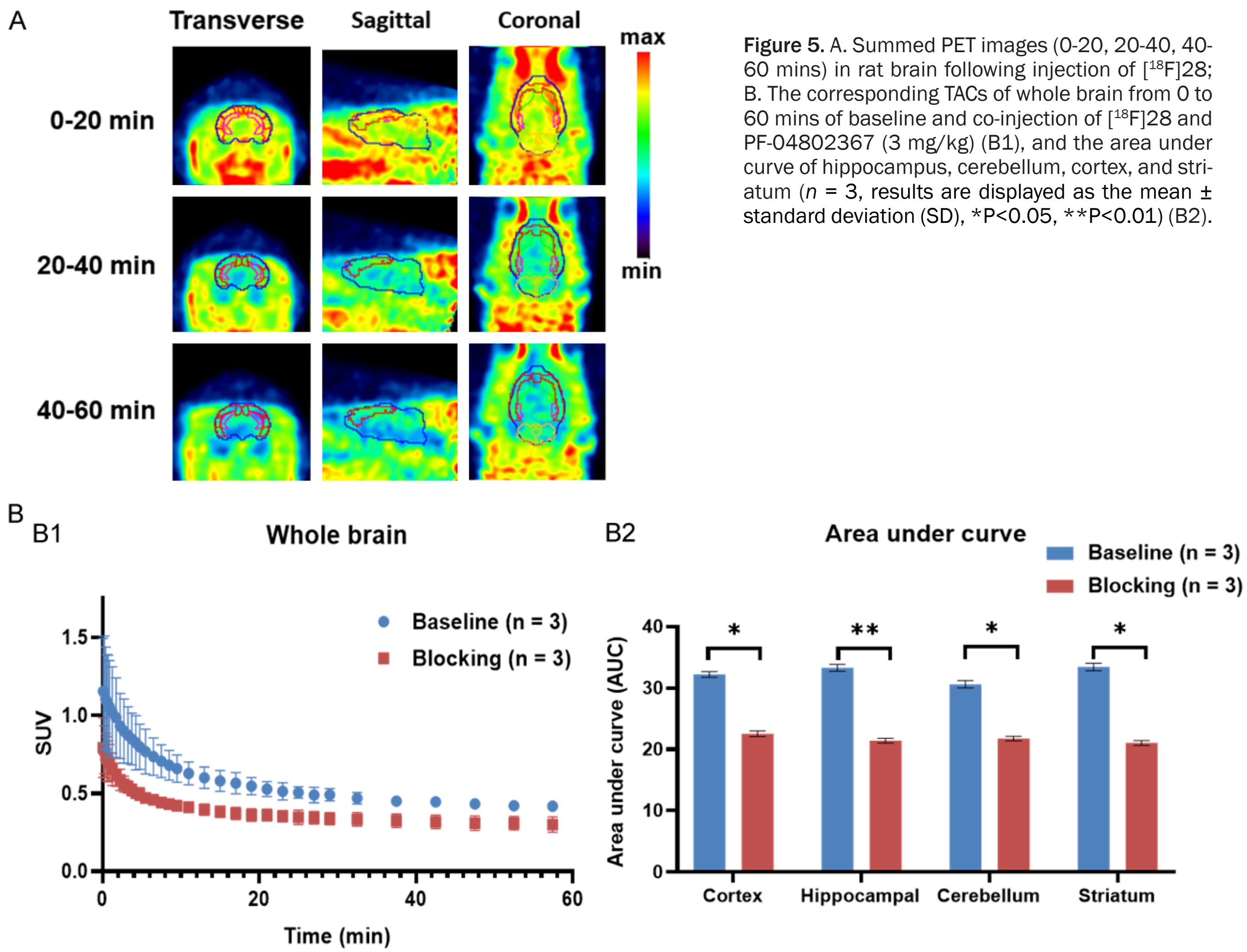

Figure 5. A. Summed PET images (0-20, 20-40, 40-60 mins) in rat brain following injection of [^{18}F]28; B. The corresponding TACs of whole brain from 0 to 60 mins of baseline and co-injection of [^{18}F]28 and PF-04802367 (3 mg/kg) (B1), and the area under curve of hippocampus, cerebellum, cortex, and striatum (*n* = 3, results are displayed as the mean ± standard deviation (SD), *P<0.05, **P<0.01) (B2).

Address correspondence to: Steven H Liang, Department of Radiology and Imaging Sciences, Emory University, Atlanta, GA 30322, USA. E-mail: steven.liang@emory.edu

References

[1] Woodgett JR. Judging a protein by more than its name: GSK-3. Sci STKE 2001; 2001: re12.

[2] Beurel E, Grieco SF and Jope RS. Glycogen synthase kinase-3 (GSK3): regulation, actions, and diseases. Pharmacol Ther 2015; 148: 114-31.

[3] Woodgett JR. Molecular cloning and expression of glycogen synthase kinase-3/factor A. EMBO J 1990; 9: 2431-8.

[4] Pei JJ, Tanaka T, Tung YC, Braak E, Iqbal K and Grundke-Iqbal I. Distribution, levels, and activity of glycogen synthase kinase-3 in the Alzheimer disease brain. J Neuropathol Exp Neurol 1997; 56: 70-8.

[5] Leroy K and Brion JP. Developmental expression and localization of glycogen synthase kinase-3β in rat brain. J Chem Neuroanat 1999; 16: 279-93.

[6] Grimes CA and Jope RS. The multifaceted roles of glycogen synthase kinase 3β in cellular signaling. Prog Neurobiol 2001; 65: 391-426.

[7] Adam RC. Regulation of cell fate in the brain by GSK3. In: Sabine WG, editors. Trends in Cell Signaling Pathways in Neuronal Fate Decision. Rijeka: IntechOpen; 2013. pp. 6.

[8] Salcedo-Tello P, Ortiz-Matamoros A and Arias C. GSK3 function in the brain during development, neuronal plasticity, and neurodegeneration. Int J Alzheimers Dis 2011; 2011: 189728.

[9] Fuster-Matanzo A, Llorens-Martín M, Sirerol-Piquer MS, García-Verdugo JM, Avila J and Hernández F. Dual effects of increased glycogen synthase kinase-3β activity on adult neurogenesis. Hum Mol Genet 2013; 22: 1300-15.

[10] Lal H, Ahmad F, Woodgett J and Force T. The GSK-3 family as therapeutic target for myocardial diseases. Circ Res 2015; 116: 138-49.

[11] McCubrey JA, Steelman LS, Bertrand FE, Davis NM, Sokolosky M, Abrams SL, Montalto G, D'Assoro AB, Libra M, Nicoletti F, Maestro R, Basecke J, Rakus D, Gizak A, Demidenko ZN, Cocco L, Martelli AM and Cervello M. GSK-3 as potential target for therapeutic intervention in cancer. Oncotarget 2014; 5: 2881-911.

[12] Azoulay-Alfaguter I, Yaffe Y, Licht-Murava A, Urbanska M, Jaworski J, Pietrokovski S, Hirschberg K and Eldar-Finkelman H. Distinct molecular regulation of glycogen synthase kinase-3α isozyme controlled by its N-terminal region: functional role in calcium/calpain signaling. J Biol Chem 2011; 286: 13470-80.

[13] Laura Sayas C, Jurado J, Avila J and Villanueva N. Structural and functional relationships between GSK3α and GSK3β proteins. Curr Biotechnol 2012; 1: 80-7.

[14] Yao HB, Shaw PC, Wong CC and Wan DC. Expression of glycogen synthase kinase-3 isoforms in mouse tissues and their transcription in the brain. J Chem Neuroanat 2002; 23: 291-7.

[15] Lau KF, Miller CC, Anderton BH and Shaw PC. Expression analysis of glycogen synthase kinase-3 in human tissues. J Pept Res 1999; 54: 85-91.

[16] Hooper C, Killick R and Lovestone S. The GSK3 hypothesis of Alzheimer's disease. J Neurochem 2008; 104: 1433-9.

[17] Gao C, Hölscher C, Liu Y and Li L. GSK3: a key target for the development of novel treatments for type 2 diabetes mellitus and Alzheimer disease. Rev Neurosci 2011; 23: 1-11.

[18] Jope RS, Yuskaitis CJ and Beurel E. Glycogen synthase kinase-3 (GSK3): inflammation, diseases, and therapeutics. Neurochem Res 2007; 32: 577-95.

[19] Martin L, Latypova X, Wilson CM, Magnaudeix A, Perrin ML, Yardin C and Terro F. Tau protein kinases: involvement in Alzheimer's disease. Ageing Res Rev 2013; 12: 289-309.

[20] Cohen P and Goedert M. GSK3 inhibitors: development and therapeutic potential. Nat Rev Drug Discov 2004; 3: 479-87.

[21] Arciniegas Ruiz SM and Eldar-Finkelman H. Glycogen synthase kinase-3 inhibitors: preclinical and clinical focus on CNS-A decade onward. Front Mol Neurosci 2022; 14: 792364.

[22] Roca C and Campillo NE. Glycogen synthase kinase 3 (GSK-3) inhibitors: a patent update (2016-2019). Expert Opin Ther Pat 2020; 30: 863-72.

[23] Georgievska B, Sandin J, Doherty J, Mörtberg A, Neelissen J, Andersson A, Gruber S, Nilsson Y, Schött P, Arvidsson PI, Hellberg S, Osswald G, Berg S, Fälting J and Bhat RV. AZD1080, a novel GSK3 inhibitor, rescues synaptic plasticity deficits in rodent brain and exhibits peripheral target engagement in humans. J Neurochem 2013; 125: 446-56.

[24] Lovestone S, Boada M, Dubois B, Hüll M, Rinne JO, Huppertz HJ, Calero M, Andrés MV, Gómez-Carrillo B, León T and del Ser T; ARGO investigators. A phase II trial of tideglusib in Alzheimer's disease. J Alzheimers Dis 2015; 45: 75-88.

[25] Rizzieri DA, Cooley S, Odenike O, Moonan L, Chow KH, Jackson K, Wang X, Brail L and Borthakur G. An open-label phase 2 study of glycogen synthase kinase-3 inhibitor LY2090314 in patients with acute leukemia. Leuk Lymphoma 2016; 57: 1800-6.

[26] O'Brien WT and Klein PS. Validating GSK3 as an in vivo target of lithium action. Biochem Soc Trans 2009; 37: 1133-8.

[27] Rong J, Haider A, Jeppesen TE, Josephson L and Liang SH. Radiochemistry for positron emission tomography. Nat Commun 2023; 14: 3257.

[28] Deng X, Rong J, Wang L, Vasdev N, Zhang L, Josephson L and Liang SH. Chemistry for positron emission tomography: recent advances in ^{11}C-, ^{18}F-, ^{13}N-, and ^{15}O-labeling reactions. Angew Chem Int Ed Engl 2019; 58: 2580-605.

[29] Vasdev N, Garcia A, Stableford WT, Young AB, Meyer JH, Houle S and Wilson AA. Synthesis and ex vivo evaluation of carbon-11 labelled N-(4-methoxybenzyl)-N'-(5-nitro-1,3-thiazol-2-yl)urea ([11C]AR-A014418): a radiolabelled glycogen synthase kinase-3β specific inhibitor for PET studies. Bioorg Med Chem Lett 2005; 15: 5270-3.

[30] Cole EL, Shao X, Sherman P, Quesada C, Fawaz MV, Desmond TJ and Scott PJ. Synthesis and evaluation of [11C]PyrATP-1, a novel radiotracer for PET imaging of glycogen synthase kinase-3β (GSK-3β). Nucl Med Biol 2014; 41: 507-12.

[31] Kumata K, Yui J, Xie L, Zhang Y, Nengaki N, Fujinaga M, Yamasaki T, Shimoda Y and Zhang MR. Radiosynthesis and preliminary PET evaluation of glycogen synthase kinase 3β (GSK-3β) inhibitors containing [11C]methylsulfanyl, [11C]methylsulfinyl or [11C]methylsulfonyl groups. Bioorg Med Chem Lett 2015; 25: 3230-3.

[32] Wang M, Gao M, Miller KD, Sledge GW, Hutchins GD and Zheng QH. The first synthesis of [^{11}C]SB-216763, a new potential PET agent for imaging of glycogen synthase kinase-3 (GSK-3). Bioorg Med Chem Lett 2011; 21: 245-9.

[33] Li L, Shao X, Cole EL, Ohnmacht SA, Ferrari V, Hong YT, Williamson DJ, Fryer TD, Quesada CA, Sherman P, Riss PJ, Scott PJ and Aigbirhio FI. Synthesis and initial in vivo studies with [11C]SB-216763: the first radiolabeled brain penetrative inhibitor of GSK-3. ACS Med Chem Lett 2015; 6: 548-52.

[34] Hu K, Patnaik D, Collier TL, Lee KN, Gao H, Swoyer MR, Rotstein BH, Krishnan HS, Liang SH, Wang J, Yan Z, Hooker JM, Vasdev N, Haggarty SJ and Ngai MY. Development of [18F]Maleimide-based glycogen synthase kinase-3β ligands for positron emission tomography imaging. ACS Med Chem Lett 2017; 8: 287-92.

[35] Liang SH, Chen JM, Normandin MD, Chang JS, Chang GC, Taylor CK, Trapa P, Plummer MS, Para KS, Conn EL, Lopresti-Morrow L, Lanyon LF, Cook JM, Richter KE, Nolan CE, Schachter JB, Janat F, Che Y, Shanmugasundaram V, Lefker BA, Enerson BE, Livni E, Wang L, Guehl NJ, Patnaik D, Wagner FF, Perlis R, Holson EB, Haggarty SJ, El Fakhri G, Kurumbail RG and Vasdev N. Discovery of a highly selective glycogen synthase kinase-3 inhibitor (PF-04802367) that modulates tau phosphorylation in the brain: translation for PET neuroimaging. Angew Chem Int Ed Engl 2016; 55: 9601-5.

[36] Bernard-Gauthier V, Mossine AV, Knight A, Patnaik D, Zhao WN, Cheng C, Krishnan HS, Xuan LL, Chindavong PS, Reis SA, Chen JM, Shao X, Stauff J, Arteaga J, Sherman P, Salem N, Bonsall D, Amaral B, Varlow C, Wells L, Martarello L, Patel S, Liang SH, Kurumbail RG, Haggarty SJ, Scott PJH and Vasdev N. Structural basis for achieving GSK-3β inhibition with high potency, selectivity, and brain exposure for positron emission tomography imaging and drug discovery. J Med Chem 2019; 62: 9600-17.

[37] Smart K, Zheng MQ, Holden D, Felchner Z, Zhang L, Han Y, Ropchan J, Carson RE, Vasdev N and Huang Y. In vivo imaging and kinetic modeling of novel glycogen synthase kinase-3 radiotracers [11C]OCM-44 and [18F]OCM-50 in non-human primates. Pharmaceuticals (Basel) 2023; 16: 194.

[38] Prabhakaran J, Sai KKS, Sattiraju A, Mintz A, Mann JJ and Kumar JSD. Radiosynthesis and evaluation of [11C]CMP, a high affinity GSK3 ligand. Bioorg Med Chem Lett 2019; 29: 778-81.

[39] Gao M, Wang M and Zheng QH. Synthesis of carbon-11-labeled isonicotinamides as new potential PET agents for imaging of GSK-3 enzyme in Alzheimer's disease. Bioorg Med Chem Lett 2017; 27: 740-3.

[40] Zhong Y, Yang S, Cui J, Wang J, Li L, Chen Y, Chen J, Feng P, Huang S, Li H, Han Y, Tang G and Hu K. Novel 18F-labeled

isonicotinamide-based radioligands for positron emission tomography imaging of glycogen synthase kinase-3β. Mol Pharm 2021; 18: 1277-84.
[41] Gundam SR, Bansal A, Kethamreddy M, Ghatamaneni S, Lowe VJ, Murray ME and Pandey MK. Synthesis and preliminary evaluation of novel PET probes for GSK-3 imaging. Sci Rep 2024; 14: 15960.
[42] Luo G, Chen L, Burton CR, Xiao H, Sivaprakasam P, Krause CM, Cao Y, Liu N, Lippy J, Clarke WJ, Snow K, Raybon J, Arora V, Pokross M, Kish K, Lewis HA, Langley DR, Macor JE and Dubowchik GM. Discovery of isonicotinamides as highly selective, brain penetrable, and orally active glycogen synthase kinase-3 inhibitors. J Med Chem 2016; 59: 1041-51.

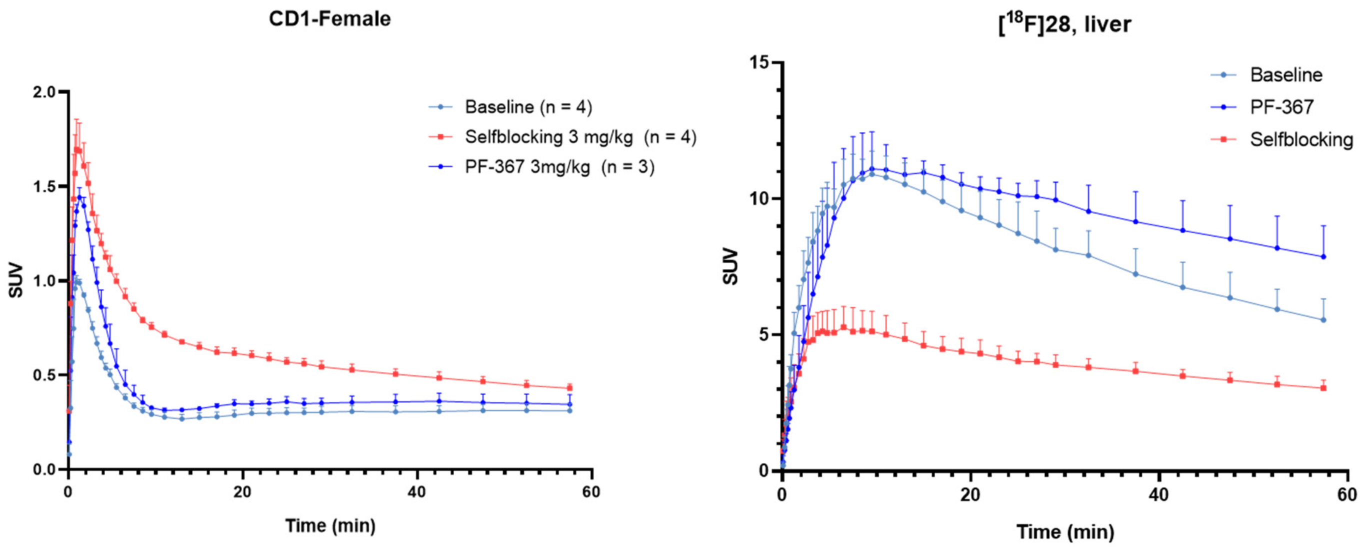

Figure S1. Summed PET images (0-20 mins) in mouse brain following injection of [[18]F]28, co-injection of [[18]F]28 and non-radioactive 28 (3 mg/kg), and co-injection of [[18]F]28 and PF-04802367 (3 mg/kg), the corresponding TACs of whole brain and liver from 0 to 60 mins.

[1]H NMR of *2-(cyclopropanecarboxamido)isonicotinic acid*

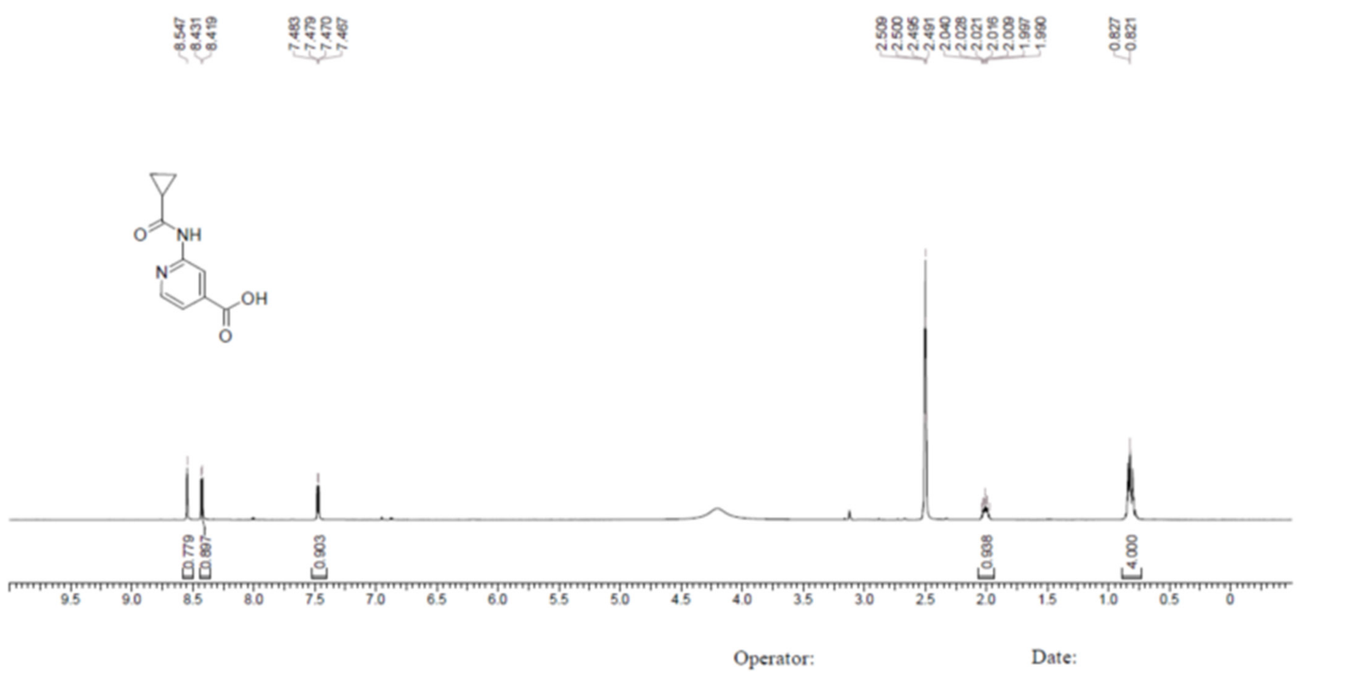

[1]H NMR of *2-(cyclopropanecarboxamido)-N-(4-(4-(4,4,5,5-tetramethyl-1,3,2-dioxaborolan-2-yl)phenyl)pyridin-3-yl)isonicotinamide*

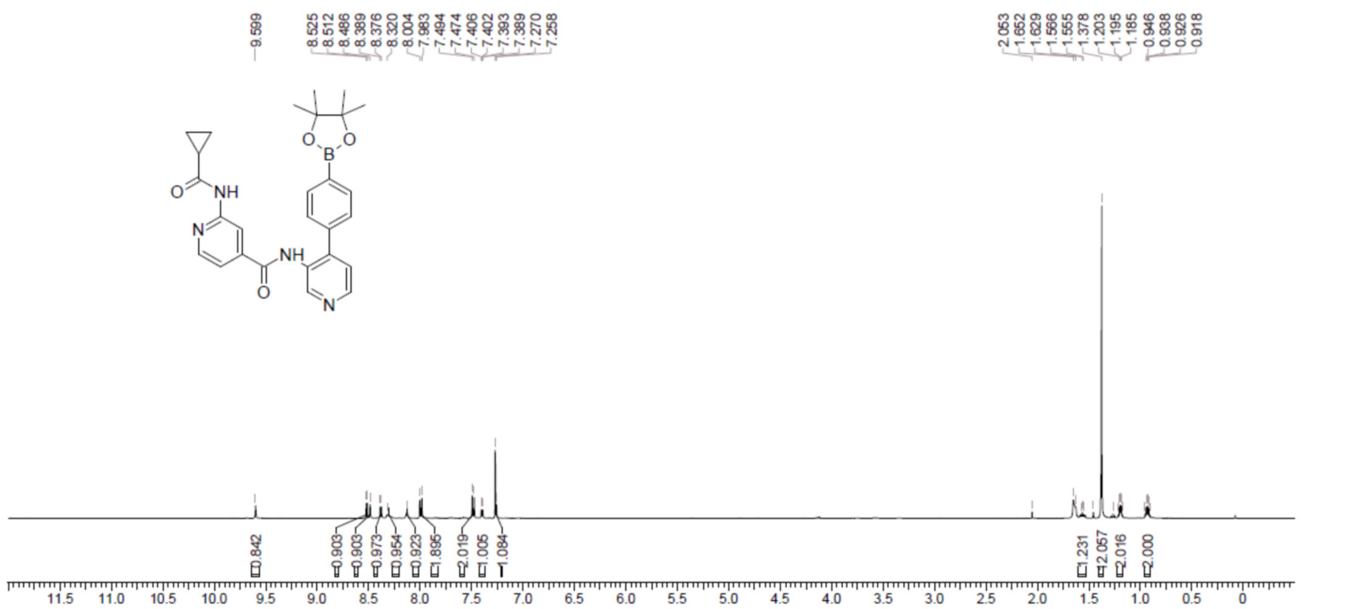

[1]H NMR of *4-(4-fluorophenyl)-3-nitropyridine*

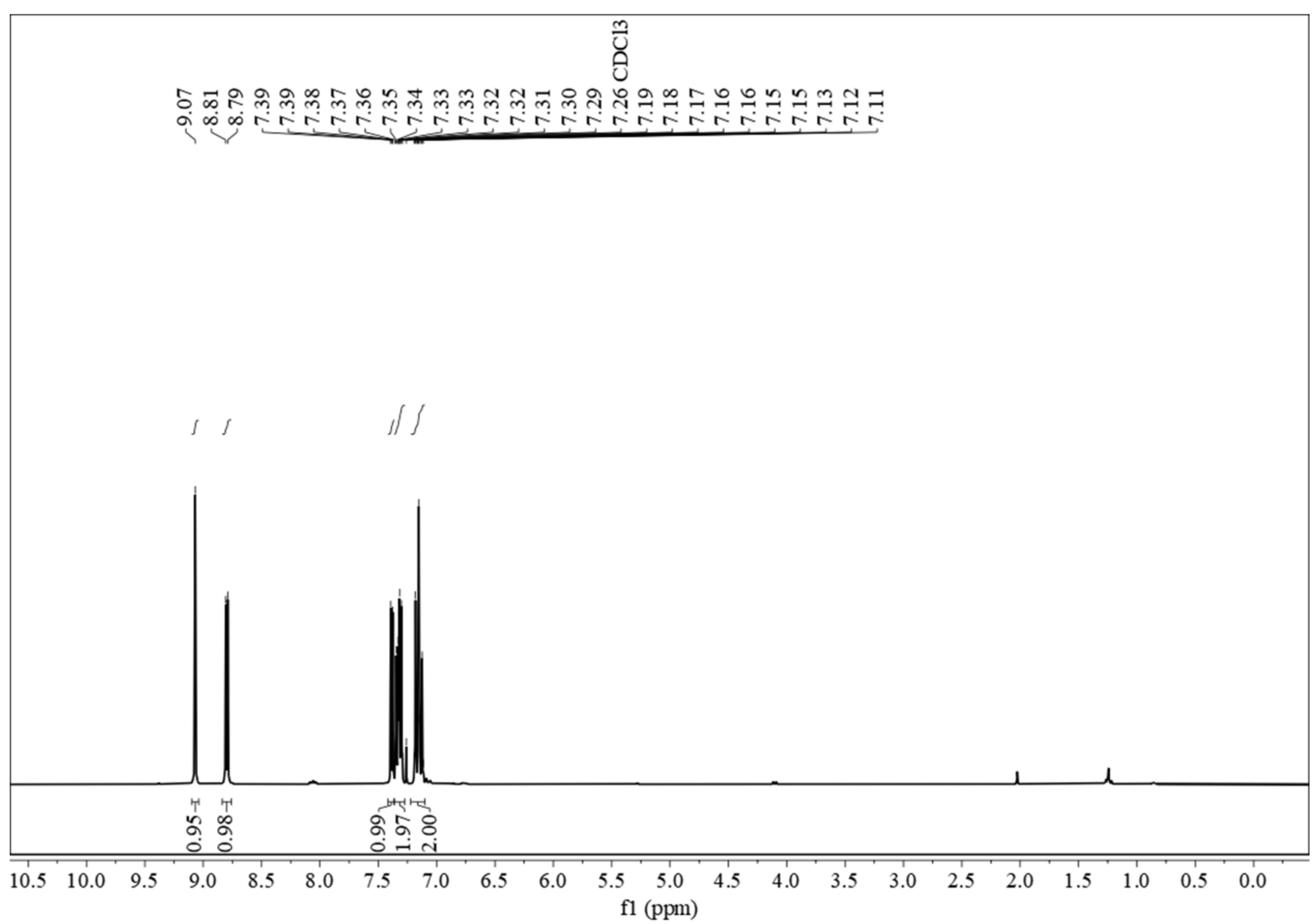

^{19}F NMR of *4-(4-fluorophenyl)-3-nitropyridine*

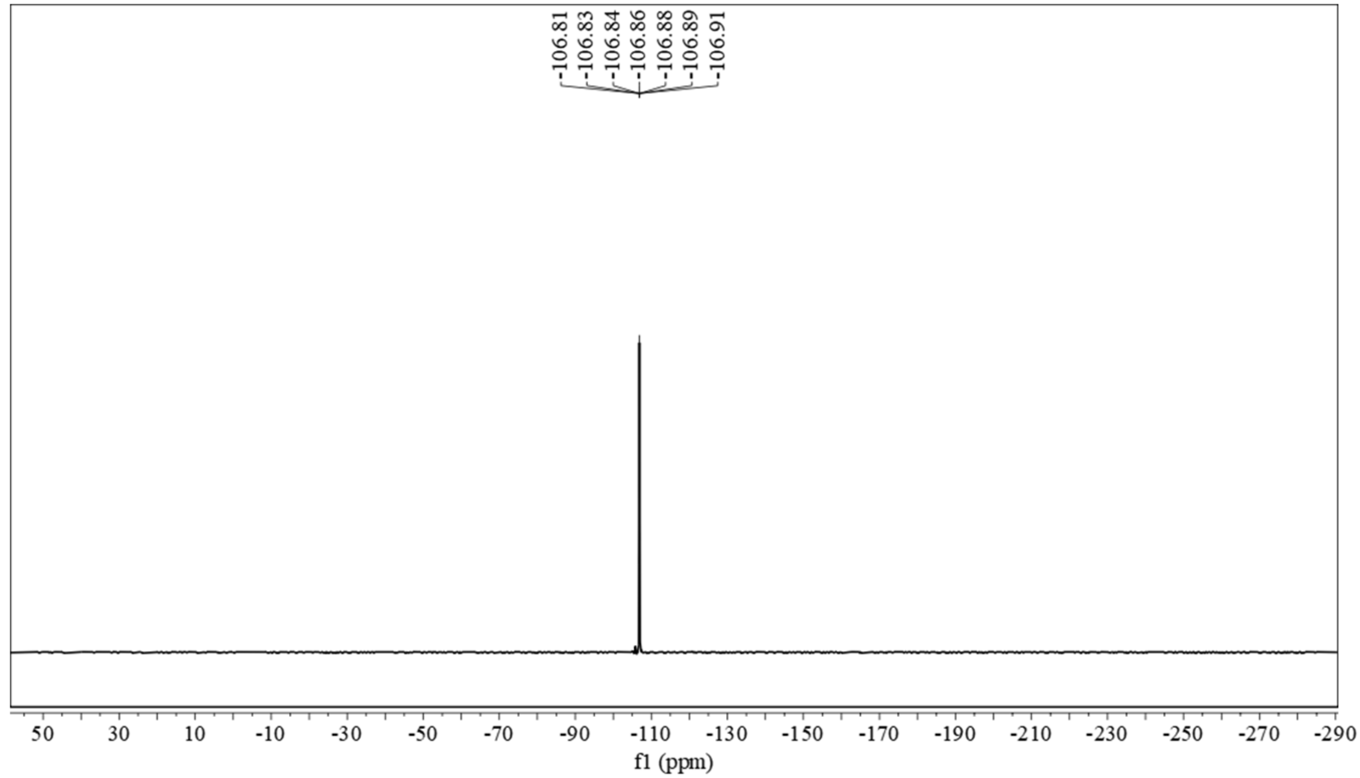

^{13}C NMR of *4-(4-fluorophenyl)-3-nitropyridine*

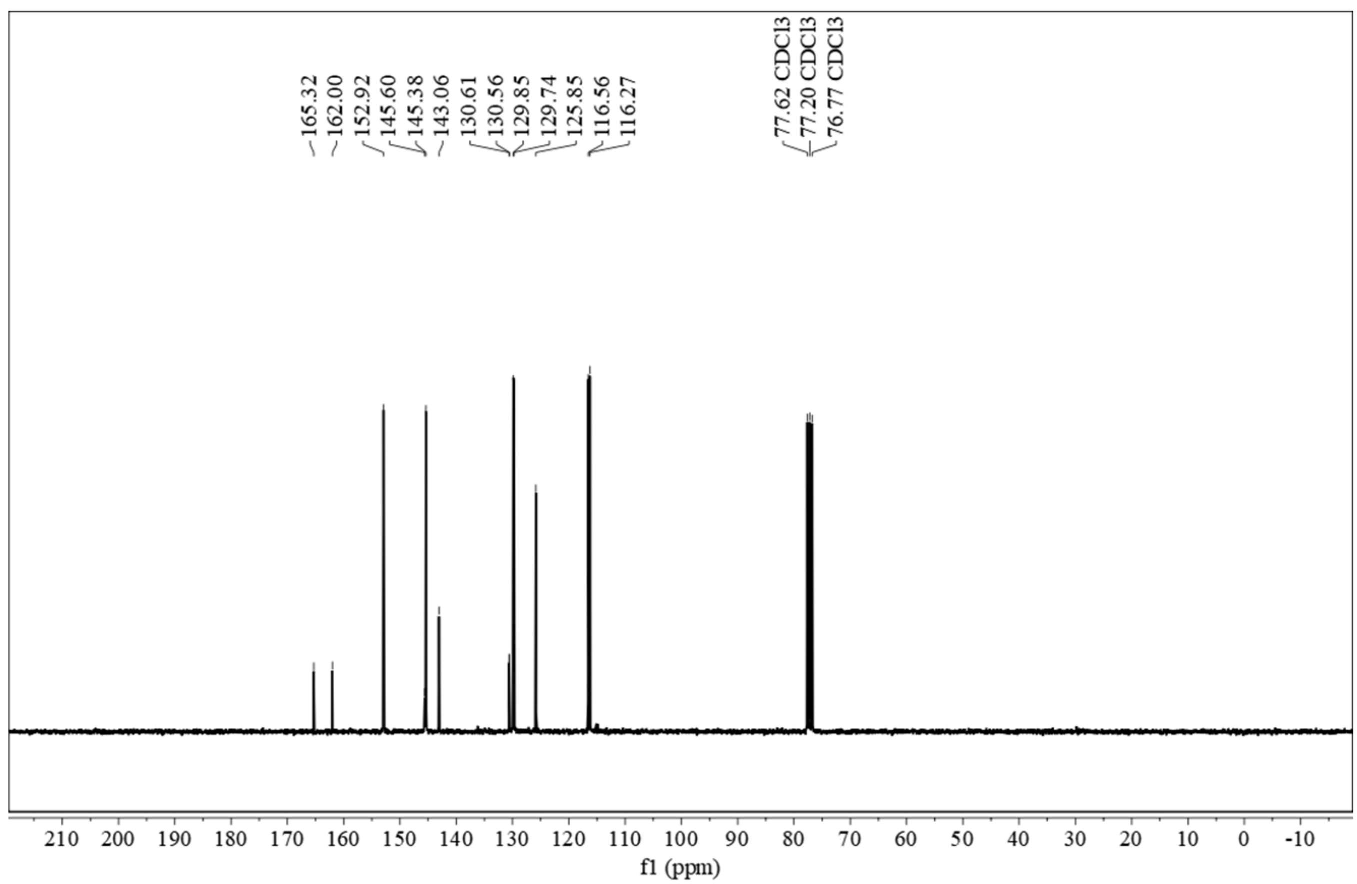

[1]H NMR of *4-(4-fluorophenyl)pyridin-3-amine*

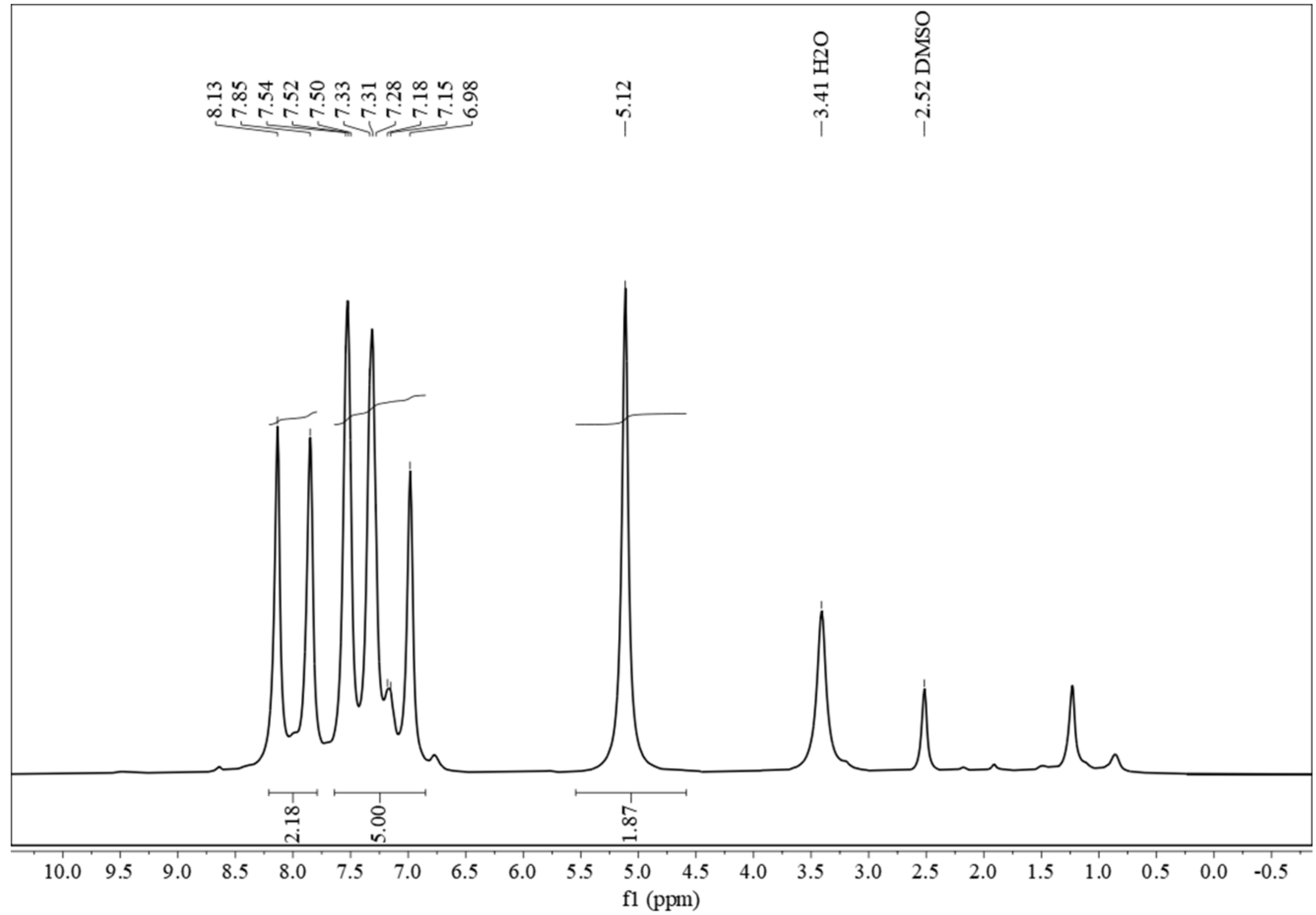

[19]F NMR of *4-(4-fluorophenyl)pyridin-3-amine*

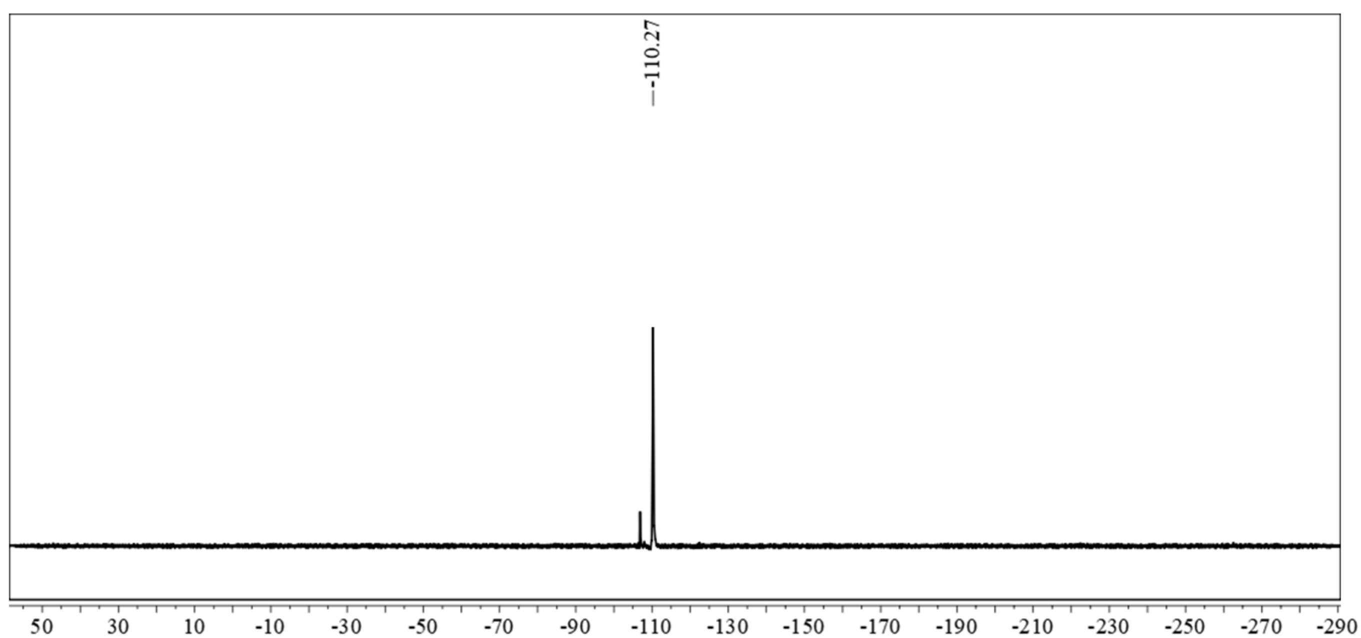

[13]C NMR of *4-(4-fluorophenyl)pyridin-3-amine*

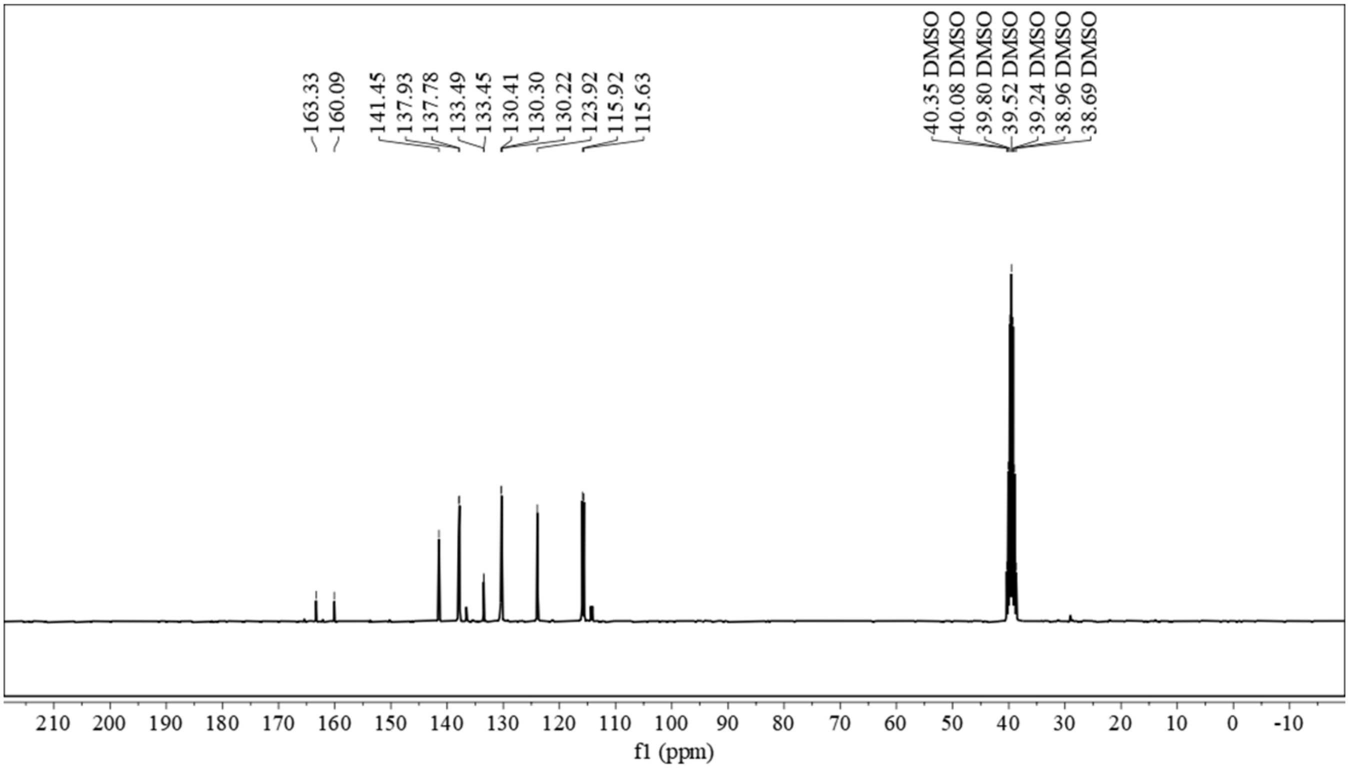

[1]H NMR of 2-(2-cyclopropyl-2-oxoethyl)-N-(4-(4-fluorophenyl)pyridin-3-yl)isonicotinamide

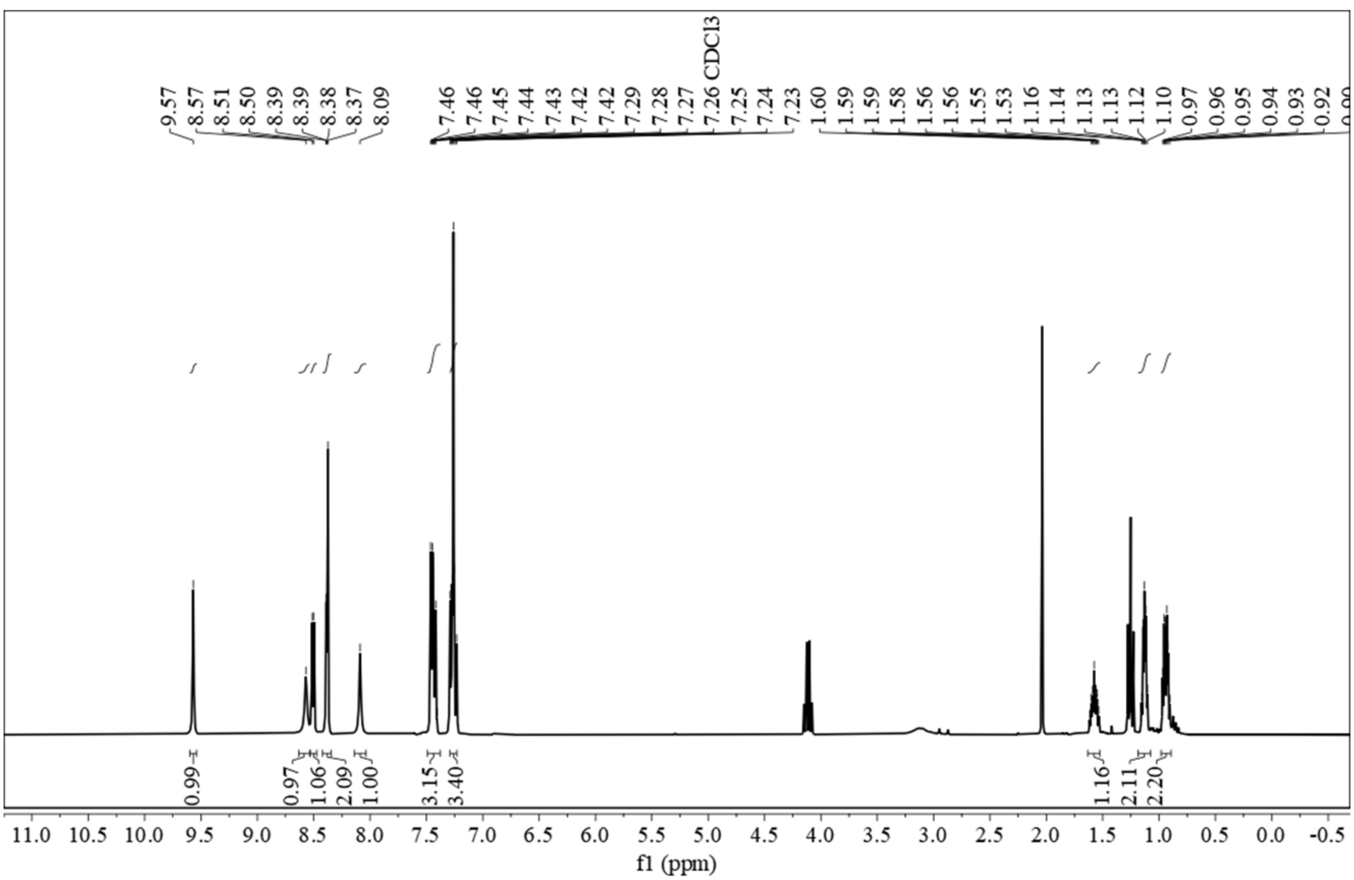

[19]F NMR of 2-(2-cyclopropyl-2-oxoethyl)-N-(4-(4-fluorophenyl)pyridin-3-yl)isonicotinamide

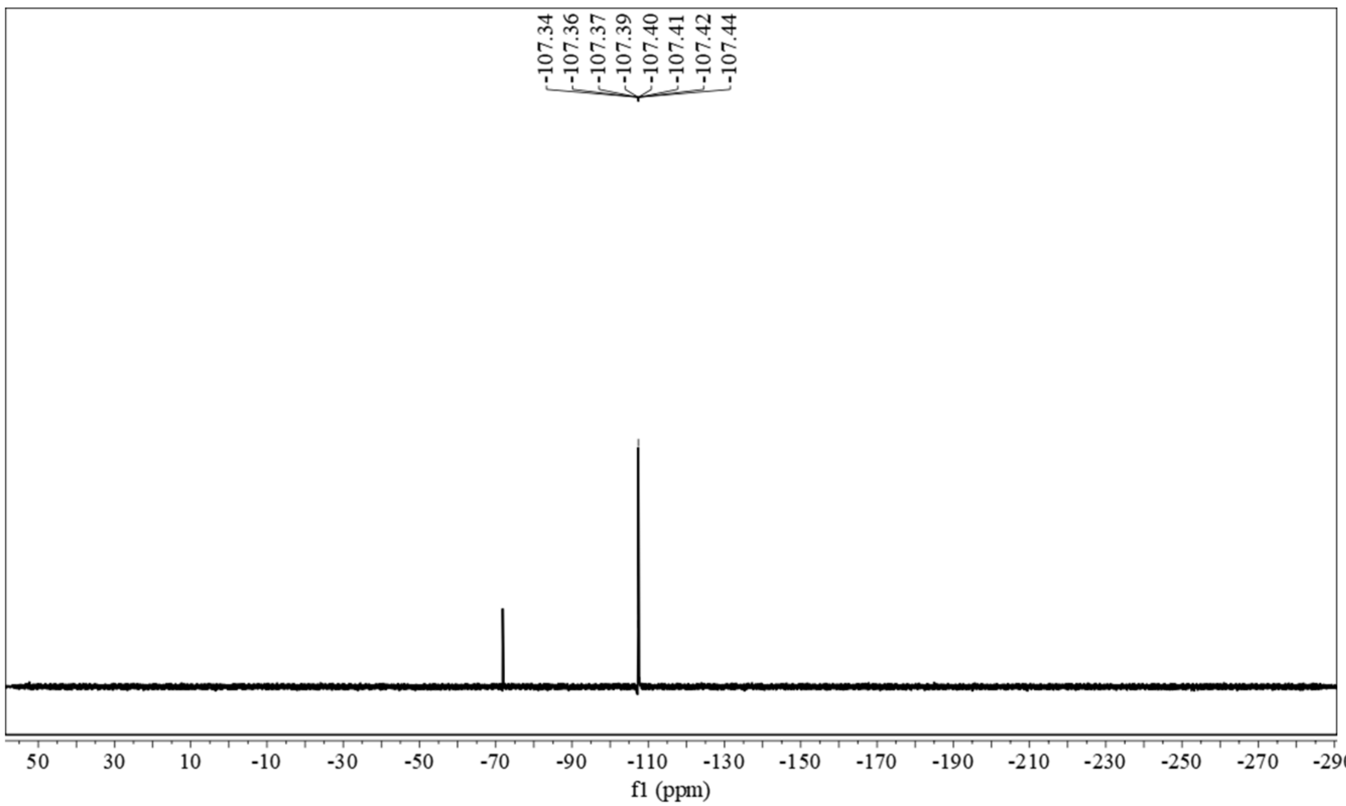

[13]C NMR of 2-(2-cyclopropyl-2-oxoethyl)-N-(4-(4-fluorophenyl)pyridin-3-yl)isonicotinamide